Journal of the Serbian Chemical Society
JSCS-info@shd.org.rs • www.shd.org.rs/JSCS

ACCEPTED MANUSCRIPT

Journal of the Serbian Chemical Society
JSCS-info@shd.org.rs • www.shd.org.rs/JSCS
J. Serb. Chem. Soc. **00(0)** 1-12 (2026)
JSCS–13775
Original scientific paper
Published DD MM, 2026

Process optimization and economic calculation of photocatalytic degradation of methylene blue over sulfur doped g-C_3N_4

WEI LI[1]*, AND SHUYU CAO[2]

[1]*Department of Economics, Heilongjiang University of Finance and Economics, Harbin 150025, China,* [2]*Department of Science and Technology, Heilongjiang University of Finance and Economics, Harbin 150025, China.*

(Received 12 February; revised 10 April; accepted 19 May 2026)

Abstract: The sulfur doping has been considered as an effective strategy to enhance the photocatalytic activity of graphitic carbon nitride (g-C_3N_4). However, there are no reports on the process optimization and economic calculation to determine the optimal photocatalytic parameters and compare the operating costs, respectively. In this work, sulfur-doped g-C_3N_4 (S/g-C_3N_4) was in situ prepared by one-pot pyrolysis approach using thiourea as the precursor and sulfur source. S/g-C_3N_4 was characterized by various instrumental techniques. Response surface methodology (RSM) was employed to determine the optimal photocatalytic conditions for the degradation of methylene blue (MB) over S/g-C_3N_4. A central composite design (CCD) with four factors at five levels was established, comprising 30 experimental runs. The optimal conditions were determined as 27.6 mg L^{-1} initial MB concentration, 4.1 g L^{-1} catalyst dosage, solution pH 8.7, and 125 min reaction time. Under these conditions, the predicted degradation efficiency could reach 99.94%, while the experimental value was 99.5%. Cost accounting indicated that the optimization substantially reduced direct costs, greatly improved equipment utilization, and enhanced operational flexibility. This work will lay the key foundation for the cost control and efficiency improvement of the scale-up application of g-C_3N_4-based photocatalyst.

Keywords: graphitic carbon nitride; photocatalyst; response surface methodology; cost accounting.

INTRODUCTION

Resource shortages and environmental pollution are closely related to our quality of life and health conditions, and have drawn high attention from governments around the world. Among the both, the issues caused by environmental pollution are more remarkable.[1] Among various kinds of

* Corresponding author. E-mail: lilidezhicheng@sina.com
https://doi.org/10.2298/JSC260212027L

environmental pollutions, organic dye wastewater has attracted the most attention because of its high concentration, many types, difficult decolorization, wide pollution and complex structure. At present, there are many technologies to treat organic dye wastewater, including adsorption, membrane separation, biodegradation, extraction, oxidation, and so on.[2] In recent years, the development of advanced oxidation technology represented by photocatalytic oxidation was the most active. The use of photocatalytic materials to purify water has become a high-tech environmental purification technology of global concern.[3]

In recent decades, a variety of novel visible light response photocatalytic materials have been developed, such as bismuth oxyhalides, metal organic frameworks, $ZnIn_2S_4$, $CuFeS_2$, WO_3, $CuWO_4$, Cu_2SnS_3, and so on. These materials have high visible light catalytic stability and activity.[4-7] However, the precious metals in the components will increase the preparation and production cost of photocatalytic materials. At the same time, they have certain toxicity and potential pollution to the water environment. Therefore, these materials are not suitable for large-scale practical applications. Graphitic carbon nitride (g-C_3N_4) is a new type of non-metallic semiconductor with a band gap of about 2.7 eV, which can achieve visible light response and make full use of solar energy. Moreover, g-C_3N_4 has stable structure, controllable performance, non-toxic and harmless nature, acid and alkali resistance, and light corrosion resistance. It has become a hot spot in the research field of photocatalytic materials.[8,9] However, the shortcomings of g-C_3N_4, such as fast electron-hole recombination and small specific surface area, limit its practical application. Therefore, heterojunction construction, doping modification, microstructure regulation and other methods have been employed to improve the photocatalytic activity of g-C_3N_4.[10,11] Among them, the doping modification with non-metallic elements could effectively change the electronic band structure of g-C_3N_4, thereby improving the photocatalytic activity.[12] Xu and coworkers successfully prepared g-C_3N_4 with nitrogen defects and sulfur doping via cold plasma technique. S-doping could offer more active sites for the photocatalytic process and enhance the stability of N defects. The visible light photocatalytic activity of S-doped g-C_3N_4 was 11.25 times higher than that of pure g-C_3N_4.[13] Ma et al. used the dielectric barrier discharge (DBD) plasma to obtain S-doped g-C_3N_4 photocatalyst under H_2S atmosphere. They found that DBD plasma treatment could make more sulfur doped into g-C_3N_4 lattice than traditional roasting approach. The as-prepared S-doped g-C_3N_4 exhibited much higher photocatalytic degradation efficiency of Rhodamine B (RhB).[14] In addition, a porous S-doped g-C_3N_4 was successfully prepared via one-step calcination method by Yang and coworkers. The as-prepared porous S-doped g-C_3N_4 displayed approximately 6.2 times higher peroxymonosulfate activation capacity for the degradation of RhB than pristine g-C_3N_4 under visible light irradiation.[15] Song et al. employed urea and thiourea as the precursors to prepare S-doped g-C_3N_4 nanosheets through physical

steam activation. The as-prepared photocatalyst exhibited 2.1 and 5.52 times higher decomposition efficiency and reaction rate for the photodegradation of methylene blue (MB) dye than bulk g-C_3N_4, respectively.[16] All in all, S doping has been proved as an efficient strategy to improve the light absorption and photogenerated electron-hole separation, consequently boosting the photocatalytic activity of g-C_3N_4.[17] However, there are few reports on the process optimization of photocatalytic degradation of organic pollutants over S-doped g-C_3N_4. Response surface methodology (RSM) based on central composite design (CCD) was a widely used process parameter optimization method.[18-20] This methodology included the experimental condition design and parameter optimization. The specific steps of this methodology can be divided into the four following aspects:[21,22] (1) determination of the variables and design of the experiment, (2) evaluation of the parameters for the mathematical model regression analysis, (3) prediction of the model response, and (4) confirmation of the accuracy of the model. In addition, as far as we know, the economic calculation of photocatalytic degradation of organic pollutants over S-doped g-C_3N_4 before and after process optimization has not been investigated.

So, in this work, S-doped g-C_3N_4 was prepared by a facile one-pot pyrolysis approach using thiourea as the precursor and sulfur source to realize the in-situ sulfur doping and achieve high photocatalytic activity. Based on the characterization analyses and photocatalytic performance evaluation of S-doped g-C_3N_4, it was the first time to employ RSM method to optimize the process of MB photodegradation over S-doped g-C_3N_4 to determine the optimal operating parameters. Moreover, the economic calculations before and after optimization were firstly implemented. Obviously, this work will lay engineering and cost foundation for the large-scale practical applications of g-C_3N_4-based photocatalyts.

EXPERIMENTAL

Preparation of S-doped g-C_3N_4

A facile one-pot pyrolysis approach was employed to in situ prepare S-doped g-C_3N_4 using thiourea as the precursor and sulfur source.[23] The specific procedures are as follows: 15 g thiourea was weighed and put into a 100 mL crucible, and then heated from room temperature to 550 °C at a heating rate of 20 °C/min in a muffle furnace. After being kept for 4 h, the sample was cooled down to room temperature in the furnace. Finally, it was ground into powder for the subsequent use.

Characterization techniques

X-ray diffraction (XRD), Fourier transform infrared spectroscopy (FTIR), field emission scanning electron microscopy (FESEM), transmission electron microscopy (TEM), and UV-vis diffuse reflectance spectroscopy (UV-vis DRS) were used to characterize the as-prepared samples. The detailed information is provided in the supplementary file.

Photocatalytic experiments

The photocatalytic performance of S-doped g-C_3N_4 was evaluated using MB dye as the target pollutant. The experimental procedure is provided in the supplementary file.

RSM optimization method

In this work, four parameters were selected as variables, namely initial MB concentration (mg L^{-1}), catalyst dosage (g L^{-1}), solution pH, and reaction time (min), which were labeled as X_1, X_2, X_3, and X_4, respectively. At the same time, the degradation rate of MB dye was used as the output response (Y). The detailed descriptions of experimental design, mathematical modeling and response optimization are provided in the supplementary file. And, the range and level of independent variables are shown in Table SI.

Economic calculation method

Generally, the standardized economic calculation for wastewater treatment process included three main parts: raw material cost, operation cost, and integrated cost.[24-26] Their calculation methods are provided in the supplementary file.

RESULTS AND DISCUSSION

Characterization of S-doped g-C_3N_4

Fig. 1A presents the XRD pattern of S-doped g-C_3N_4 sample. The XRD pattern shows two prominent diffraction peaks located at 2θ=13° and 27.5°. The peak at 13° belongs to the in-plane ordering of triazine units and is indexed to the (100) crystal plane of g-C_3N_4, whereas the peak at 27.5° corresponds to interlayer stacking of aromatic layers and is assigned to the (002) crystal plane of g-C_3N_4 .[27] The FT-IR spectrum of S-doped g-C_3N_4 is displayed in Fig. 1B. The absorption bands in the 1225-1640 cm^{-1} region are assigned to stretching vibrations of C–N and C=N bonds within the N-containing ring framework, together with exocyclic C–N stretching.[28] The broad band at 3135 cm^{-1} is associated with N–H stretching vibrations,[29] while the band at 796 cm^{-1} is attributed to bending vibration of the C–N ring.[30]

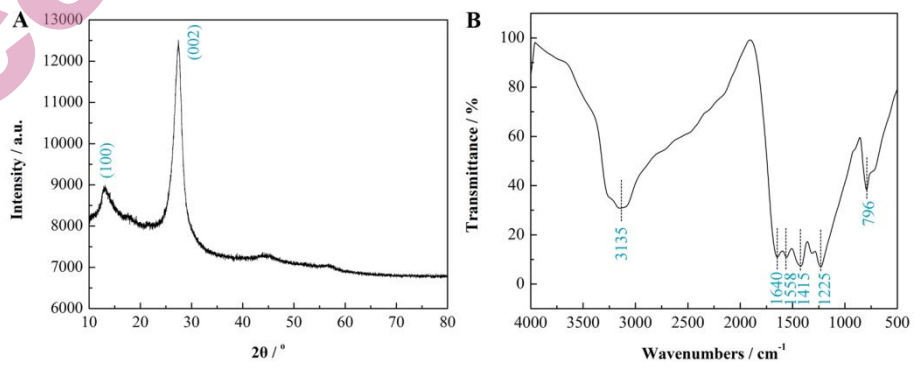

Fig. 1. (A) XRD pattern and (B) FTIR spectrum of S-doped g-C_3N_4.

Fig. 2A gives an FESEM image of S-doped g-C_3N_4, displaying a non-uniform particulate morphology in which the particles are irregularly agglomerated, consistent with the typical morphology of g-C_3N_4.[31] Fig. 2B shows a TEM image of the S-doped g-C_3N_4 sample. It can be seen that the as-prepared sample has a typical thin-layer structure with a certain wrinkle, similar to graphene. This thin layer structure will further increase the specific surface area of the S-doped g-C_3N_4 sample, thereby improving the adsorption capacity and photocatalytic activity of the sample.[32] From the energy dispersive spectrum (EDS) of S-doped g-C_3N_4 (Fig. 2C), it can be clearly seen that the as-prepared sample contain three main elements of C, N, and S, which indicates that S has been successfully introduced into g-C_3N_4. In addition, no characteristic diffraction peak or absorption peak belonging to S was found in XRD pattern and FTIR spectrum, which implied that S might enter into the crystal structure of g-C_3N_4 and replace the position of C or N, rather than the form of impurities.[13-16]

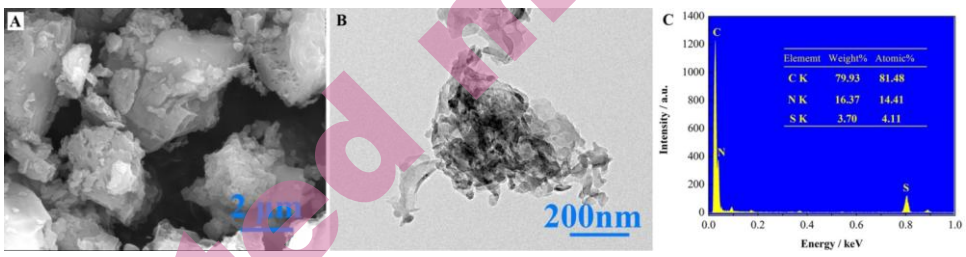

Fig. 2. (A) FESEM, (B) TEM, and (C) EDS images of S-doped g-C_3N_4.

Fig. 3A shows the UV-vis DRS spectrum of S-doped g-C_3N_4, from which it can be observed that the S-doped g-C_3N_4 sample has strong visible-light absorption and the absorption edge is located at approximately 412 nm. According to the extrapolation of $[F(R)\cdot h\upsilon]^{1/2}$ curve versus photon energy hυ (Fig. 3B), the band gap (E_g) of S-doped g-C_3N_4 is estimated to be 2.63 eV, in agreement with literature reports.[33] Notably, the as-prepared sample exhibits an additional absorption feature near 645 nm in the UV-vis DRS spectrum, corresponding to an E_g of 1.81 eV. This might be associated with S-induced impurity energy level in the band structure,[34] which can facilitate the enhancement of photocatalytic performance.

Process optimization of MB photodegradation over S-doped g-C_3N_4

To evaluate the photocatalytic performance of S-doped g-C_3N_4, MB with analytical purity was used as the target pollutant under the conditions of 10 mg L^{-1} MB, 5.0 g L^{-1} S-doped g-C_3N_4, pH=7, and room temperature. As shown in Fig. 4A, after 60 min in the dark to reach adsorption equilibrium, the removal rate of MB is only 9.4%, suggesting that the contribution of adsorption to MB removal can be neglected. While, after 120 min of photocatalytic irradiation, the corresponding degradation rate can be increased to 95.8%. Accordingly, the as-

prepared S-doped g-C_3N_4 sample exhibits stronger photocatalytic performance towards MB degradation. Additionally, this photocatalytic process follows the pseudo-first-order kinetic model (Fig. 4B), with a reaction rate constant of 0.02296 min^{-1}. The UV-vis absorption spectra of the MB solution during different photocatalytic periods are presented in Fig. 4C, where we can see that the main absorption peak of the MB dye molecule at 650 nm disappeared after 120 min of photocatalytic reaction, indicating that the dye molecule has been decomposed. And, the removal percentage of total organic carbon (TOC) after 120 min photocatalytic irradiation was measured as 78.4%. So, it can be supposed that the MB dye was decomposed into CO_2, H_2O, and other small-molecular substances.

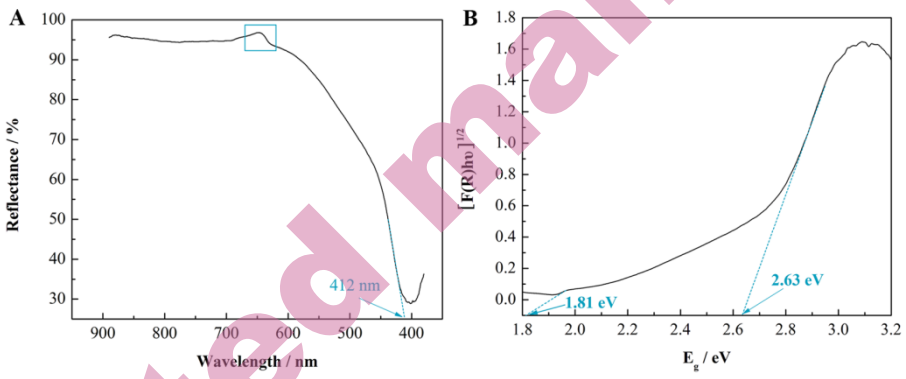

Fig. 3. (A) UV-vis DRS spectrum and (B) $[F(R)\cdot h\upsilon]^{1/2}$ versus hυ curve of S-doped g-C_3N_4.

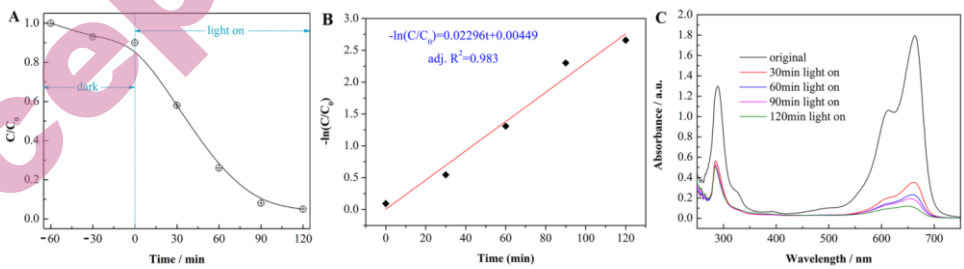

Fig. 4. (A) Photocatalytic performance towards MB degradation over S-doped g-C_3N_4; (B) fitting line of pseudo-first-order kinetic model; (C) UV-vis absorption spectra of the MB solution during different photocatalytic periods.

Based on the above results, the effects of different experimental parameters on the degradation rate of MB dye were evaluated by RSM. According to the CDD, an experimental scheme with 4 factors and 5 levels was designed, and a total of 30 sets of experiments were carried out. The CDD experimental matrix is listed in Table SII, along with the experimental and predicted values of Y response. Among

them, six groups of experiments are repeated ones at the center point, which ensures that the relative error of the experiment is small. Their closer response values mean the higher experimental accuracy.[35]

To predict the response value, the experimental values were fitted by second-order polynomial regression, and the results are shown in Equation (1):

$$Y = 66.46 + 5.82X_1 - 13.35X_2 + 7.62X_3 + 12.70X_4 - 2.74X_1X_2 + 1.69X_1X_3 + 1.70X_1X_4 + 0.79X_2X_3 + 0.21X_2X_4 - 1.17X_3X_4 - 2.48X_1^2 - 3.90X_2^2 - 10.22X_3^2 - 2.61X_4^2 \quad (1)$$

From the analysis of variance (ANOVA) (Table SIII), we can know that the F value is 8.09, which is much higher than the standard value $F_{0.05}$=2.42, which means that the second-order polynomial used is highly significant. In addition, as listed in Table SII, the experimental and predicted values of Y response are relatively close, with the correlation coefficient of R^2=0.9588. This is the main criterion for evaluating the correlation between the experimental and predicted values.[36]

Moreover, the predicted response values are in good agreement with the experimental values (Fig. S2). And, the Prob>F value is less than 0.0500, which means that the influence of the variable is significant, and this value is greater than 0.1000, indicating that the influence of the variable is not significant.[37] Therefore, in this work, it can be seen from Table SIII that X_1, X_2, X_3, X_4, X_1X_3, X_1X_4, X_1^2, X_3^2, and X_4^2 are the significant influencing variables during the MB photodegradation over S-doped g-C_3N_4. In addition, the statistical analysis of the experimental data indicate that the initial MB dye concentration, S-doped g-C_3N_4 dosage, solution pH, and reaction time have significant effect on MB photodegradation.

The three-dimensional (3D) response surface diagrams of the interaction effect between two factors are shown in Fig. 5, including the interactions between initial MB concentration and S-doped g-C_3N_4 dosage, initial MB concentration and solution pH, initial MB concentration and reaction time, S-doped g-C_3N_4 dosage and solution pH, S-doped g-C_3N_4 dosage and reaction time, and solution pH and reaction time. It can be seen that the degradation rate of MB increases with the decrease of the initial MB concentration and the increase of the S-doped g-C_3N_4 dosage (Fig. 5A); increases with the decrease of the initial MB concentration and the increase of the solution pH (Fig. 5B); increases with the decrease of the initial MB concentration and the increase of the reaction time (Fig. 5C); increases with the increase of the S-doped g-C_3N_4 dosage and the solution pH (Fig. 5D); increases with the increase of the S-doped g-C_3N_4 dosage and the reaction time (Fig. 5E); and increases with the increase of the reaction time and the solution pH (Fig. 5F). According to the prediction model, the process parameters of MB photodegradation over S-doped g-C_3N_4 photoctatalyst are optimized as follows:

the initial MB concentration is 27.6 mg L^{-1}, S-doped g-C_3N_4 dosage is 4.1 g L^{-1}, solution pH is 8.7, and reaction time is 127 min. Under this optimal condition, the predicted degradation rate of MB can reach 99.94 %. Under the identical conditions, the experimental value of MB degradation rate is 99.5 %, showing excellent agreement with the model prediction.

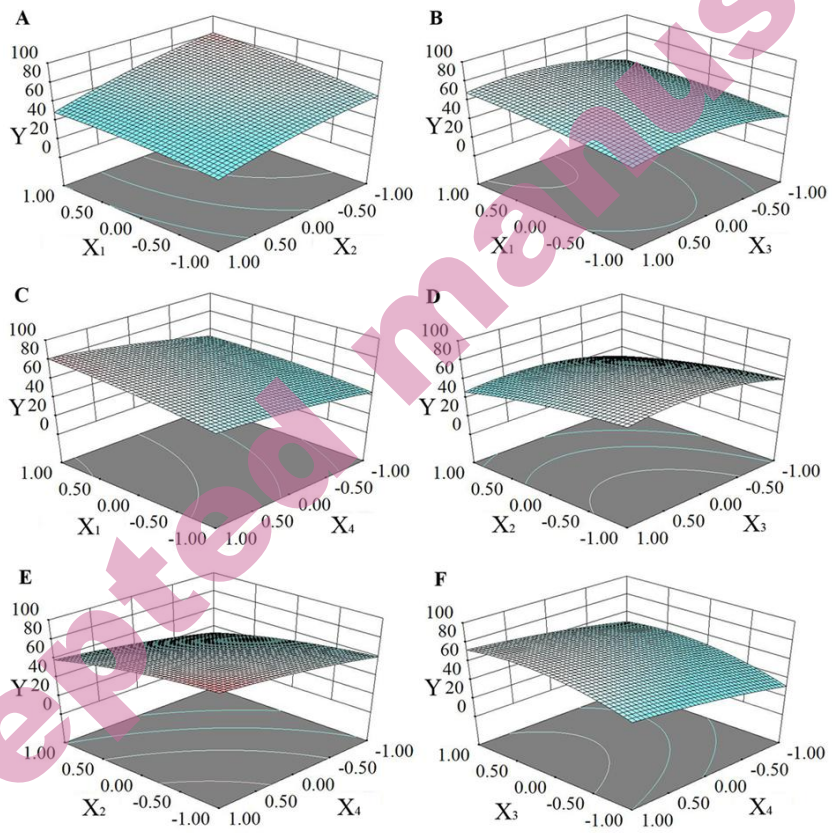

Fig. 5. 3D response surface of MB photodegradation (Y) over S-doped g-C_3N_4 with the interaction effect between (A) initial MB concentration (X_1) and S-doped g-C_3N_4 dosage (X_2), (B) initial MB concentration (X_1) and solution pH (X_3), (C) initial MB concentration (X_1) and reaction time (X_4), (D) S-doped g-C_3N_4 dosage (X_2) and solution pH (X_3), (E) S-doped g-C_3N_4 dosage (X_2) and reaction time (X_4), and (F) solution pH (X_3) and reaction time (X_4).

Economic calculation of MB photodegradation over S-doped g-C_3N_4

(1) Comparative analysis of raw material cost

Table SIV provides the comparative analysis data of raw material cost before and after optimization. Before optimization, the catalyst cost for treating 1 m^3 MB wastewater was 5 kg × 80 CNY kg^{-1} = 400 CNY. After optimization, the corresponding cost for treating 1 m^3 MB wastewater was 4.1 kg × 80 CNY kg^{-1} =

328 CNY. Therefore, the catalyst cost for treating 1 m^3 wastewater was reduced by 72 CNY, with a decrease of 17.8 %. Moreover, after optimization, the pH value of MB solution was adjusted from 7.0 to 8.7, so sodium hydroxide needed to be added to adjust the pH value. Based on the calculation of the acid-alkaline balance, 0.12 kg sodium hydroxide was required to adjust the pH value from 7.0 to 8.7 of 1 m^3 wastewater, and the corresponding cost was 0.12 kg × 2.5 CNY kg^{-1} = 0.3 CNY. After optimization, although the acid-alkaline adjustment cost was slightly increased, combined with the significant reduction of catalyst cost, the integrated raw material cost still achieved a net saving of 71.7 CNY for treating 1 m^3 wastewater, with a reduction by 17.7 %.

(2) Comparative analysis of operation cost

Table SV gives the comparative analysis data of operation cost before and after optimization. The energy consumption of photocatalytic reaction mainly came from xenon lamp (300 W) and stirrer (50 W). The energy consumption was positively correlated with the reaction time. Before optimization, the energy consumption for treating 1 m^3 wastewater was (300W + 50W) × 3h = 1.05 kWh, and the corresponding energy cost was 1.05 kWh × 0.6 CNY kWh^{-1} = 0.63 CNY. After optimization, the reaction time was 127 min (2.12 h). So, the energy consumption for treating 1 m^3 wastewater was (300W + 50W) × 2.12 h = 0.742 kWh, and the corresponding energy cost was 0.742 kWh × 0.6 CNY kWh^{-1} = 0.445 CNY. Therefore, after optimization, the energy consumption cost for treating 1 m^3 wastewater was reduced by 0.185 CNY, with a decrease of 29.4%.

With regard to the labor cost, before optimization, assuming that the operation time of single batch treatment of 1 m^3 wastewater was about 3.5 h, the labor cost was 3.5 h × 30 CNY h^{-1} = 105 CNY. After optimization, the operation time was shortened to 2.5 h, and the labor cost was 2.5 h × 30 CNY h^{-1} = 75 CNY. Therefore, the labor cost for treating 1 m^3 wastewater was directly reduced by 30 CNY, with a decrease of 28.6 %.

(3) Comparative analysis of integrated cost

Based on the raw material and operation costs, the integrated cost for treating 1 m^3 MB wastewater was calculated. Before optimization, the integrated cost for treating 1 m^3 MB wastewater was (400 + 0 + 0.63 + 105) CNY= 505.63 CNY. While, after optimization, the integrated cost for treating 1 m^3 MB wastewater was (328 + 0.3 + 0.445 + 75) CNY = 403.745 CNY. So, after optimization, the integrated cost for treating 1 m^3 MB wastewater was reduced by 101.885 CNY, with a decrease of 20.0 %.

CONCLUSION

In this work, S-doped g-C_3N_4 was successfully prepared by a facile one-step pyrolysis approach, using thiourea as the precursor and sulfur source. The as-prepared sample was characterized by XRD, FTIR, FESEM, TEM, EDS, and UV-

vis DRS. The sample exhibited wide visible-light absorption region, and its E_g was estimated to be 2.63 eV. Furthermore, an additional absorption feature near 645 nm could be seen in the UV-vis DRS spectrum, corresponding to an E_g of 1.81 eV. This might be associated with S-induced impurity energy level in the band structure. The as-prepared sample exhibited stronger photocatalytic performance towards MB degradation. After 120 min of photocatalytic irradiation, the MB degradation rate could be increased to 95.8%. Based on RSM under CDD, the process optimization of MB photodegradation over S-doped g-C_3N_4 photoctatalyst was conducted. Based on the economic cost calculations, after optimization, the integrated cost for the photodegradation of 1 m^3 MB wastewater over S-doped g-C_3N_4 was reduced from 505.63 to 403.745 CNY, with a decrease of 20.0 %.

SUPPLEMENTARY MATERIAL

Additional data are available electronically at the pages of journal website: https://www.shd-pub.org.rs/index.php/JSCS/article/view/13775, or from the corresponding author on request.

И З В О Д

ОПТИМИЗАЦИЈА ПРОЦЕСА И ЕКОНОМСКИ ПРОРАЧУН ФОТОКАТАЛИТИЧКЕ ДЕГРАДАЦИЈЕ МЕТИЛЕНСКОГ ПЛАВОГ КОРИШЋЕЊЕМ g-C_3N_4 ДОПИРАНОГ СУМПОРОМ

WEI LI[1] и SHUYU CAO[2]

[1]*Department of Economics, Heilongjiang University of Finance and Economics, Harbin 150025, China,* [2]*Department of Science and Technology, Heilongjiang University of Finance and Economics, Harbin 150025, China.*

Допирање сумпором сматра се ефикасном стратегијом за побољшање фотокаталитичке активности графитног угљеничног нитрида (g-C_3N_4). Међутим, у литератури нису присутни извештаји о оптимизацији овог процеса, као ни о економском прорачуну при одређивању оптималних фотокаталитичких параметара. У овом раду, g-C_3N_4 допиран сумпором (S/g-C_3N_4) припремљен је in situ методом пиролизе у једном кораку, уз коришћење тиоурее као прекурсора и извора сумпора. У раду је извршена карактеризација S/g-C_3N_4 различитим инструменталним техникама. За одређивање оптималних фотокаталитичких услова за деградацију метиленског плавог (MB) коришћењем S/g-C_3N_4 коришћена је метода одзивне површине (RSM). Успостављен је дизајн експеримента са четири фактора на пет нивоа, који је обухватио 30 експерименталних понављања. Добијени су следећи оптимални услови: почетна концентрација MB од 27,6 mg L^{-1}, доза катализатора 4,1 g L^{-1}, pH раствора 8,7 и време реакције 125 min. Под овим условима, предвиђена ефикасност деградације достиже 99,94%, док је експериментална вредност износила 99,5%. Анализа трошкова показала је да оптимизација значајно смањује директне трошкове, у великој мери побољшава искоришћеност опреме и повећава оперативну флексибилност. Овај рад поставља кључну основу за контролу трошкова и повећање ефикасности при примени фотокатализатора на бази g-C_3N_4 у индустријским размерама.

(Примљено 12. фебруара; ревидирано 10. априла; прихваћено 19. маја 2026.)

REFERENCES

1. X. Z. Tang, Y. M. Xin, R. H. Chen, X. F. Ren, L. G. Gao, H. Xu, P. X. Yang, A. M. Liu, *J. Mater. Chem. A* **13** (2025) 34122-34148 (https://doi.org/10.1039/d5ta04748j)
2. G. Kavitha, M. Govindhan, S. Premkumar, *J. Water Process Eng.* **80** (2025) 109071 (https://doi.org/10.1016/j.jwpe.2025.109071)
3. M. S. N. Awang, B. L. Phoon, W. M. A. W. Daud, S. Boonyuen, J. C. Juan, *Mater. Sci. Eng. B-Adv. Funct. Solid-State Mater.* **324** (2026) 119025 (https://doi.org/10.1016/j.mseb.2025.119025)
4. X. S. Wang, Z. Y. Yuan, *Coord. Chem. Rev.* **548** (2026) 217184 (https://doi.org/10.1016/j.ccr.2025.217184)
5. M. Q. Xiao, J. J. Kong, W. J. Wang, B. Yang, S. Q. Guo, *J. Alloy. Compd.* **1046** (2025) 184670 (https://doi.org/10.1016/j.jallcom.2025.184670)
6. J. Avinash, G. Madhumitha, S. M. Roopan, *J. Environ. Chem. Eng.* **13** (2025) 118368 (https://doi.org/10.1016/j.jece.2025.118368)
7. M. W. Xu, Y. J. Wu, X. Z. Zhao, J. Wang, G. C. Jiang, S. Li, Z. Q. Li, *J. Alloy. Compd.* **1042** (2025) 184188 (https://doi.org/10.1016/j.jallcom.2025.184188)
8. M. G. Sahini, A. Parmain, I. Onoka, S. F. Mwanga, *J. Alloy. Compd.* **1044** (2025) 183642 (https://doi.org/10.1016/j.jallcom.2025.183642)
9. N. Farooq, N. Qureshi, S. Hussain, A. M. Qureshi, Z. Sattar, R. K. Manavalan, N. Ullah, M. K. Aslam, *Int. J. Hydrog. Energy* **180** (2025) 151763 (https://doi.org/10.1016/j.ijhydene.2025.151763)
10. H. Noreen, A. Farooq, S. Naz, N. Amjed, A. Ahmad, A. Aftab, S. Muzammal, *J. Iran. Chem. Soc.* **22** (2025) 1659-1682 (https://doi.org/10.1007/s13738-025-03252-6)
11. M. Zheng, M. R. Guo, F. Ma, W. W. Li, Y. J. Shao, *Nanoscale Adv.* **7** (2025) 4780-4802 (https://doi.org/10.1039/d5na00439j)
12. C. Wen, Z. W. Xie, X. X. Gao, L. Q. Feng, Z. H. Li, P. C. Li, A. L. Wang, J. Wang, W. Q. Yao, *Colloids Surf. A-Physicochem. Eng. Asp.* **727** (2025) 138402 (https://doi.org/10.1016/j.colsurfa.2025.138402)
13. H. L. Xu, X. F. Peng, J. X. Zheng, Z. Wang, *Front. Chem. Sci. Eng.* **17** (2023) 93-101 (https://doi.org/10.1007/s11705-022-2175-x)
14. L. Ma, S. Z. Hu, P. Li, Q. Wang, H. F. Ma, W. Li, *J. Phys. Chem. Solids* **118** (2018) 166-171 (https://doi.org/10.1016/j.jpcs.2018.03.017)
15. D. Yang, L. Zhao, X. T. Feng, L. L. Ma, H. M. Ding, *Funct. Mater. Lett.* **14** (2021) 2151019 (https://doi.org/10.1142/S179360472151019X)
16. W. L. Song, N. N. Zhang, X. J. Ma, X. T. Liu, D. N. Li, J. Li, *Chemistryselect* **9** (2024) e202400279 (https://doi.org/10.1002/slct.202400279)
17. M. X. Zuo, X. Y. Li, Y. S. Liang, F. X. Zhao, H. B. Sun, C. Liu, X. M. Gong, P. F. Qin, H. Wang, Z. B. Wu, L. Luo, *Sep. Purif. Technol.* **308** (2023) 122875 (https://doi.org/10.1016/j.seppur.2022.122875)
18. D. M. Azar, A. Feizbakhsh, H. A. Panahi, A. Niazi, *Int. J. Environ. Anal. Chem.* **102** (2022) 8490-8502 (https://doi.org/10.1080/03067319.2020.1853114)
19. C. Y. Chen, Z. F. Luo, H. X. Tu, X. J. Lin, Y. W. Pang, J. F. Huang, J. Zhang, X. J. Wang, Q. Y. Cai, Z. B. Wei, J. Zeng, J. Qiu, *J. Hazard. Mater.* **486** (2025) 136986 (https://doi.org/10.1016/j.jhazmat.2024.136986)
20. H. M. Samuel, C. A. Mecha, M. M. M'Arimi, *React. Kinet. Mech. Catal.* **137** (2024) 2415-2430 (https://doi.org/10.1007/s11144-024-02650-w)

21. N. Szpisjak-Gulyás, A. N. Al-Tayawi, Z. H. Horváth, Z. László, S. Kertész, C. Hodúr, *Acta Aliment.* **52** (2023) 521-537 (https://doi.org/10.1556/066.2023.00235)
22. C. E. Aristizabal-Alzate, E. Castillejos-López, A. B. Dongil, M. Romero-Sáez, *Chemistryopen* **14** (2025) 202400148 (https://doi.org/10.1002/open.202400148)
23. H. Zhao, L. C. Wu, H. Y. Xu, *Sci. Adv. Mater.* **8** (2016) 1408-1416 (https://doi.org/10.1166/sam.2016.2731)
24. M, Budych-Gorzna, L. Jaroszynski, P. Oleskowicz-Popiel, *J. Environ. Chem. Eng.* **9** (2021) 106366 (https://doi.org/10.1016/j.jece.2021.106366)
25. M. Yao, Z. Ju, Z. Ran, T. Chen, H. Pan, *J. Water Process Eng.* **69** (2025) 106626 (https://doi.org/10.1016/j.jwpe.2024.106626)
26. K. Wu, S. Y. Li, F. Jiang, J. Wang, G. L. Liu, G. H. Chen, *Water Sci. Technol.* **68** (2013) 530-536 (https://doi.org/10.2166/wst.2013.247)
27. J. Yang, X. Zhang, C. Xie, Ji. Long, Y. Wang, L. Wei, X. Yang, *J. Electron. Mater.* **50** (2021) 1067-1074 (https://doi.org/10.1007/s11664-020-08654-1)
28. Q. H. Shen, C. Y. Wu, Z. Y. You, F. L. Huang, J. S. Sheng, F. Zhang, D. Cheng, H. Yang, *J. Mater. Res.* **35** (2020) 2148-2157 (https://doi.org/10.1557/jmr.2020.182)
29. G. Nabi, N. Malik, W. Raza, *Inorg. Chem. Commun.* **119** (2020) 108050 (https://doi.org/10.1016/j.inoche.2020.108050)
30. S. Challagulla, S. Payra, C. Chakraborty, S. Roy, *Phys. Chem. Chem. Phys.* **21** (2019) 3174-3183 (https://doi.org/10.1039/C8CP06855K)
31. Y. C. Ren, T. Gong, S. L. Tan, M. Chen, F. Zhou, Y. Lin, L. Yang, Q. Peng, *J. Alloy. Compd.* **902** (2022) 163752 (https://doi.org/10.1016/j.jallcom.2022.163752)
32. L. F. Wang, Z. Y. Fan, X. X. Cao, P. F. Fan, Y. Xie, Q. Sun, J. S. Zhao, *Nanomaterials* **12** (2022) 2569 (https://doi.org/10.3390/nano12152569)
33. A. M. Li, X. H. Cong, H. T. Qin, W. C. Xu, X. H. Zhang, W. Z. Wang, F. Guo, *New J. Chem.* **47** (2023) 3910-3920 (https://doi.org/10.1039/D2NJ06154F)
34. L. Dong, H. W. Chu, S. P. Xu, Y. Li, S. Z. Zhao, D. C. Li, *Nanophotonics* **11** (2022) 139-151 (https://doi.org/10.1515/nanoph-2021-0549)
35. B. Hernández, C.G. Blázquez, V. Aristizábal-Marulanda, M. Martín, *Ind. Eng. Chem. Res.* **59** (2020) 16720-16729 (https://doi.org/10.1021/acs.iecr.0c03336)
36. D. H. Zhang, J. W. Liu, H. Wang, Y. Y. Wang, *Environ. Res.* **290** (2026) 123449 (https://doi.org/10.1016/j.envres.2025.123449)
37. K.-J. Wang, P.-S. Wang, *J. Water Process Eng.* **78** (2025) 108703 (https://doi.org/10.1016/j.jwpe.2025.108703).